ISSN 1344-8803, CSSE-2 May 1, 1999

Multi-Objective Multirate Control Design with Applications to Frequency Dividing Cooperative Control[1][2]

Hiroshi Ito[†3]

[†]Department of Control Engineering and Science, Kyushu Institute of Technology
680-4 kawazu, Iizuka, Fukuoka 820-8502, Japan
Phone: (+81)948-29-7717, Fax: (+81)948-29-7709
E-mail: hiroshi@ces.kyutech.ac.jp

Abstract: This paper addresses a multi-objective approach to multirate control design taking account of diverse characteristics of composing systems and disturbances. Explicit formulas are derived to deal with multiple continuous-time performance objectives in multirate sampled-data control design. The applicability and usefulness of the multi-objective multirate control are illustrated by an example of a tracking problem of a double cart system which has redundant degrees of freedom. It is shown that the multi-objective approach to multirate design fits frequency dividing cooperative control well and it gives a useful guideline on how to choose suitable sampling and hold periods within a required level of control performance.

Key Words: Multirate control, Sampled-data control, Sampling rates, Multi-objective control, Tracking problem, Redundant degree of freedom, $\mathcal{H}^\infty$ control

---

[1]Technical Report in Computer Science and Systems Engineering, Log Number CSSE-2, ISSN 1344-8803.

[2]The first version of the paper was completed by May 7, 1997, and the current version of the paper was completed by January 6, 1998.

[3]Author for correspondence

1 Introduction

Many systems have redundant degrees of freedom to perform desired control. For example, an arm system of the human has two degrees of freedom to move the hand to a right position. One freedom is the shoulder joint. The other is the elbow joint. We rarely use the shoulder joint when we raise and lower the hand quickly. The shoulder, however, is not good at short-distance and precise movement. The elbow joint is quicker in action although it can generate less amount of work than the shoulder joint. This two-link structure of the arm efficiently creates a quick and precise position control system which can afford a required amount of work. This strategy of dividing the control roles among several freedoms are very useful in practical engineering. In frequency domain, this control strategy is nothing but dividing the frequency band of tracking control into several pieces. For the two-link example, the shoulder joint is responsible for low frequency components of the command input signal. On the other hand, the elbow is in charge of high frequencies. Thus, an appilcation of appropriate division of frequency bands to redundant degrees of freedom creates a clever cooperative control system. The author refers to the control strategy as frequency dividing cooperative control(FDCC).

An FDCC system was designed in Sampei *et al.* (1991) using $\mathcal{H}^\infty$ control theory. Position control of a double cart system was considered, where one cart moves on the surface of the other cart. The control objective is to make the upper cart track the reference signal of its absolute position. The force driving each cart is available as a control input. The lower cart is heavier than the upper one. Sampei *et al.* (1991) obtained a controller as a continuous-time system. Needless to say, the controller has to be discretized to be implemented as a practical sampled-data system. In Sampei *et al.* (1991), the discretization was regarded as an approximation of a continuous-time control system.

Any sampled-data system has AD/DA converters. A question arising here is what the most reasonable choice of sampling and holding frequency is. In an FDCC system, since frequency bands of signals are separated, there could be a choice of multiple frequencies of sampling and holding determined appropriately for the frequency ranges of individual signals. In the case of the two-link robot arm, the shoulder link does not require fast sampling frequency while the elbow does. For the double cart tracking control system, a faster frequency of changing the control input might not be suitable for the actuator of the heavy lower cart. This is why this paper focuses on multirate control of systems having redundant degrees of freedom. This paper shows practical usefulness of multi-rate control via the FDCC.

Multiple rates in a sampled-data control system are useful in many cases. Sensors and actuators might determine a physically allowable sampling and holding frequency. For example, some measurements are only infrequently available specially in chemical industry. Since aerospace systems often include phenomena covering a wide range of characteristic frequencies, instrumentation measurements are available at multiple rates(Glasson, 1983). More simply, unnecessary high rates for low-bandwidth signals just wastes microprocessing power(Semba, 1993). A multirate control structure accommodates these situations.

In a multi-input, multi-output(MIMO) control system having multiple loops, largest time constant involved in one loop may be quite different from that in the other loops. It may be advisable to sample and hold slowly in a loop involving a large time constant, while in a loop involving only small time constants the rate must be fast. Thus, different rates are used in different feedback paths. A classical frequency domain approach to such an MIMO control design is the successive loop closure. The faster loop is closed first, which is called the inner-

loop. Then the outer-loop (slow) loop is closed with a slower sampling and hold rate(Franklin *et al.*, 1990). Therefore, we see that frequencies are decomposed in the design. However, this successive loop closure has a drawback of ignoring cross coupling and outer-loops in the design of the inner-loop. The achieved performance can be significantly inferior to that achieved by direct MIMO design considering the entire system together. It is not until the design comes to the slowest outer- loop that an accurate performance can be predicted. Moreover, the performance is only measured in discrete time of the slowest sampling rates.

For multirate systems, stability and performance analysis based on continuous-time signals becomes very important since signals operating with different sampling and hold periods interact each other through the governing continuous-time system. Unlike single-rate systems, multirate systems have relativity of sampling and hold periods. Continuous-time performance analysis is necessary to give a fair judgment for every signal and to appreciate the effectiveness of multirate control correctly. To suggest multirate control rather than single-rate one, design methods have to be able to take advantage of multirate control. Recently, sampled-data control theory taking account of intersample behavior has gained much attention (For example, Kabamba and Hara (1993), Yamamoto (1994), Bamieh and Pearson (1992), Hayakawa *et al.* (1994), Araki *et al.* (1996) and Sun *et al.* (1992) to name a few). Voulgaris and Bamieh (1993) presented a complete solution to $\mathcal{H}^\infty$ control problem for multirate sampled-data systems(See Ito *et al.* (1995) for correction). Chen and Qiu (1994) also reported a similar result. Those papers, however, only deal with single objective control problems. When we have to consider several requirements in several frequency ranges and when there are several disturbances and perturbations to be evaluated separately, it is natural to consider multiple performance objectives. Approaches to single objective control are no longer directly applicable to this kind of control problems.

This paper proposes a procedure for dealing with multiple objectives in multirate control synthesis. This paper also shows how to formulate the frequency dividing cooperative control(FDCC) of a multirate sampled-data system as an $\mathcal{L}^2$-induced norm multi-objective minimizing problem and solve it in state space. Then, it will be demonstrated that the multirate control yields sufficiently good performance as an FDCC system using appropriately chosen sampling and hold frequencies. Our standpoint is that it is not clever to design a sampled-data system which has unnecessarily fast sampling and hold frequencies.

The paper is organized as follows: In Section 2, a multirate control system to be considered is introduced and the $\mathcal{L}^2$-induced norm suboptimal multi-objective control problem with the decay rate constraint is stated. In Section 3, a mathematical transformation of the original problem into a discrete-time equivalent taking account of multiple objectives is newly developed. In Section 4, the transformation is successfully used to propose a design method of developing multi-objective multirate controllers. In Section 5, the multi-objective approach to multirate control design is applied to an FDCC design of a double cart system. First, the control objective of the FDCC is stated. Then, the section shows how the FDCC problem is reduced to an $\mathcal{L}^2$-induced norm multi-objective constrained minimizing problem. The method proposed in Section 4 is used to solve the problem. The design illustrates the effectiveness of the multi-objective approach to multirate control design. It also demonstrates practical usefulness of the multirate strategy in an FDCC design.

In the sequel, ℓ denotes the space of one-sided sequences defined on the set of nonnegative integers. ℓ_n is the space of one-sided sequences of n-dimensional real vectors. The dimension is dropped if it is clear from the context. $\mathcal{L}^\nu$ denotes Banach space of all measurable functions

(vector-valued) on the time set $[0,\infty)$ which are ν-integrable. $\|H\|_{\mathcal{B}(\mathcal{L}^\nu)}$ is $\mathcal{L}^\nu$-induced norm of H on $\mathcal{L}^\nu$. $\|H\|_\infty$ denotes $\mathcal{H}^\infty$-norm of proper real-rational functions (matrices) of z which have no poles outside the open unit disk. If H is a function of s, $\|H\|_\infty$ is $\mathcal{H}^\infty$-norm of proper real-rational functions (matrices) which have no poles in the closed right half plane. $\mathcal{F}_\ell(\cdot,\cdot)$ denotes lower linear fractional transformation. I_n is an identity matrix of the dimension n. Some parts of this paper originally appeared as conference papers(Ito *et al.*, 1996; Teraoka *et al.*, 1997).

2 Multi-objective Multirate Control

Consider the multirate sampled-data system shown in Fig.1, which is denoted by $\Sigma[\boldsymbol{G}, \mathcal{HCS}]$. Here, $w := [w_1^T, w_2^T]^T$ is the exogenous input, $z := [z_1^T, z_2^T]^T$ is the controlled output, and both signals are continuous-time. u is the control input, y is the measurement output, and both signals are discrete-time. $\boldsymbol{G}$ denotes the plant that is a finite-dimensional linear time-invariant(FDLTI) continuous-time system. $\mathcal{HCS}$ is a linear, causal, multirate sampled-data controller, where $\mathcal{S}$ is the multirate sampler defined by

$$\begin{aligned} &\mathcal{S} := \mathrm{diag}[\mathcal{S}_1, \mathcal{S}_2, \cdots, \mathcal{S}_p] \\ &y_i = \mathcal{S}_i y_{c\,i}\,, \quad y_i(l) = y_{c\,i}(lL_iT), \quad i = 1,2,...,p\ . \end{aligned} \tag{1}$$

The signal $y_{c\,i}$ is a continuous-time signal of dimension e_i. A positive integer E denotes the size of the output vector $y = [y_1^T, y_2^T, \cdots, y_p^T]^T$ and there holds $E = \sum_{i=1}^p e_i$. The operator $\mathcal{H}$ represents the multirate hold (zero-order):

$$\begin{aligned} &\mathcal{H} := \mathrm{diag}[\mathcal{H}_1, \mathcal{H}_2, \cdots, \mathcal{H}_m]\,, \quad u_{c\,j} = \mathcal{H}_j u_j \\ &u_{c\,j}(k(K_jT)+t) = u_j(k), \ \ 0 < t \le K_jT, \ \ j = 1,2,...,m\ , \end{aligned} \tag{2}$$

where $u_{c\,j}$ is a continuous-time signal of dimension f_j. L_i and K_j are positive integers. The size of the input vector $u = [u_1^T, u_2^T, \cdots, u_m^T]^T$ is $F = \sum_{j=1}^m f_j$. Let N be the least common multiple among L_i $(i = 1,2,\ldots,p)$ and K_j $(j = 1,2,\ldots,m)$. Then define $P_i := N/L_i$ and $M_j := N/K_j$ for $i = 1,2,\ldots,p$ and $j = 1,2,\ldots,m$. We partition the plant $\boldsymbol{G}$ as

$$\begin{bmatrix} z \\ y_c \end{bmatrix} = \begin{bmatrix} \boldsymbol{G}_{11} & \boldsymbol{G}_{12} \\ \boldsymbol{G}_{21} & \boldsymbol{G}_{22} \end{bmatrix} \begin{bmatrix} w \\ u_c \end{bmatrix}\ . \tag{3}$$

Assume that the plant $\boldsymbol{G}$ is described as

$$\begin{aligned} \dot{x} &= Ax + B_1 w + B_2 u_c \\ z &= C_1 x + D_{11} w + D_{12} u_c \\ y_c &= C_2 x\ . \end{aligned} \tag{4}$$

in the state space. We refer to (A, B_j, C_i, D_{ij}) for the state-space realization of $\boldsymbol{G}_{ij}$. We partition B_1 as

$$B_1 = [B_1^1 \quad B_1^2]\ ,$$

which are compatible in size with the partition of the vector $w = [w_1^T, w_2^T]^T$. In the same manner, we write

$$C_1 = \begin{bmatrix} C_1^1 \\ C_1^2 \end{bmatrix}\ ,\ D_{12} = \begin{bmatrix} D_{12}^1 \\ D_{12}^2 \end{bmatrix}\ ,\ D_{11} = \begin{bmatrix} D_{11}^{11} & D_{11}^{12} \\ D_{11}^{21} & D_{11}^{22} \end{bmatrix}$$

so that they are compatible with the output $z = [z_1^T, z_2^T]^T$. We assume that (A, B_2) is stabilizable and that (C_2, A) is detectable. The common sampling period NT is supposed to be nonpathological, i.e., whenever δ is an eigenvalue of A with nonnegative real part, none of the points $\delta + j2\pi k/NT, k \neq 0$ is an eigenvalue of A.

Let $M = \sum_{j=1}^{m} M_j f_j$ and a discrete-time lifting operator $W_M : \ell_F \to \ell_M$ is defined as follows:

$$\hat{u} = \{\hat{u}(k)\}_{k=0}^{\infty} = W_M c = \left\{ \begin{bmatrix} u_1(0) \\ u_1(1) \\ \vdots \\ u_1(M_1-1) \\ u_2(0) \\ \vdots \\ u_m(M_m-1) \end{bmatrix}, \begin{bmatrix} u_1(M_1) \\ u_1(M_1+1) \\ \vdots \\ u_1(2M_1-1) \\ u_2(M_2) \\ \vdots \\ u_m(2M_m-1) \end{bmatrix}, \dots \right\}, \tag{5}$$

where

$$u = \left\{ \begin{bmatrix} u_1(0) \\ u_2(0) \\ \vdots \\ u_m(0) \end{bmatrix}, \begin{bmatrix} u_1(1) \\ u_2(1) \\ \vdots \\ u_m(1) \end{bmatrix}, \dots \right\}. \tag{6}$$

Here, $\hat{u}$ is the discrete-time lifted input signal. Let $P = \sum_{i=1}^{p} P_i e_i$ and we define a discrete-time lifting operator $W_P : \ell_E \to \ell_P$ in the same manner as W_M. Here, $\hat{y} := W_P y$ is the lifted sequence of the output signal y. For details of the lifting, we refer the reader to Ito *et al.* (1994), Ito *et al.* (1995) and Meyer (1990). The set of (M_j, P_i)-shift-varying operators is defined by

$$\mathcal{L}_{SV}(M_j, P_i) := \left\{ H : \text{linear operator } \ell_p \to \ell_m \ , \ \left(\sum_{j=1}^{m} S_j^{M_j} \right) H = H \left(\sum_{i=1}^{p} S_i^{P_i} \right) \right\}, \tag{7}$$

where S_j denotes the right shift operator on the jth component of the signal vector. It is assumed that the controller $\boldsymbol{C}$ belongs to $\mathcal{L}_{SV}(M_j, P_i)$ and that it is causal and finite-dimensional. To put it another way,

$$\boldsymbol{C} \in \left\{ \begin{array}{l} \boldsymbol{C} \ : (M_j, P_i)\text{-causal}, \ \boldsymbol{C} = W_M^{-1} \hat{\boldsymbol{C}} W_P, \\ \hat{\boldsymbol{C}} \ \text{is finite-dimensional, linear shift-invariant} \end{array} \right\}. \tag{8}$$

Note that if the operator $\hat{\boldsymbol{C}}$ is a finite-dimensional linear shift-invariant(FDLSI) system whose direct-feedthrough matrix of the state-space realization satisfies (M_j, P_i)-causality conditions, $W_M^{-1} \hat{\boldsymbol{C}} W_P$ always belongs to $\mathcal{L}_{SV}(M_j, P_i)$ and it is (M_j, P_i)-causal (Ito *et al.*, 1994; Meyer, 1990). We refer to the state of the minimal state-space realizations of $\hat{\boldsymbol{C}}$ as the state of the controller $\boldsymbol{C}$. Let $x_k(q), q = 0, 1, 2, \dots$ denote the state of the controller $\boldsymbol{C}$.

The multirate control system $\Sigma[\boldsymbol{G}, \mathcal{H}\boldsymbol{C}\mathcal{S}]$ shown in Fig.1 is said to be continuous-time internally stable if there exist positive real constants α_c, κ_c such that the associated unforced system satisfies

$$\|x(t)\| \leq \|X(0)\| \kappa_c e^{-\alpha_c t} \ ; \ \forall t \geq 0 \tag{9}$$

$$\|x_k(q)\| \leq \|X(0)\| \kappa_c e^{-\alpha_c q NT} \ ; \ \forall q = 0, 1, 2, \dots \tag{10}$$

for any initial state $X(0) = [x(0)^T, x_k(0)^T]^T$. The continuous-time internal stability describes not only a property of an unforced system, but also an input-output property of a system with

hybrid external signals. The system $\Sigma[\boldsymbol{G}, \mathcal{HC}\,\mathcal{S}]$ is said to be $\mathcal{L}^\nu$ hybrid stable if the operator mapping (w, v, r) to (z, y, u) is bounded from $\mathcal{L}^\nu \times \ell^\nu \times \ell^\nu$ to $\mathcal{L}^\nu \times \ell^\nu \times \ell^\nu$ in Fig.2. Here, ν is any number in $[1, \infty]$. The internal stability can be rephrased in terms of $\mathcal{L}^\nu$ hybrid stability, (See Ito *et al.* (1995) and Ito *et al.* (1994) for details).

Theorem 1 *The following statements are equivalent for any* $\nu \in [1, \infty]$.
(i) $\Sigma[\boldsymbol{G}, \mathcal{HC}\,\mathcal{S}]$ *is continuous-time internally stable.*
(ii) $\Sigma[\boldsymbol{G}, \mathcal{HC}\,\mathcal{S}]$ *is* $\mathcal{L}^\nu$ *hybrid stable.*

The following theorem clarifies the equivalence between continous-time internal stability and discrete-time internal stability. It is important that the decay rate of the state transition of $\Sigma[\boldsymbol{G}, \mathcal{HC}\,\mathcal{S}]$ can be predicted precisely by the discrete decay rate.

Theorem 2 *Suppose that* α_d *is a positive real number. There exists a positive real number* κ_d *such that the state transition of* $\Sigma[\boldsymbol{G}, \mathcal{HC}\,\mathcal{S}]$ *with* $w \equiv 0$ *satisfies*

$$\|x(qNT)\| \le \|X(0)\|\kappa_d e^{-\alpha_d q}, \quad \|x_k(q)\| \le \|X(0)\|\kappa_d e^{-\alpha_d q}, \quad \forall q = 0, 1, 2, \ldots \tag{11}$$

for any initial state $X(0) = [x(0)^T, x_k(0)^T]^T$ *if and only if there exists a positive real number* κ_c *such that the state transition satisfies*

$$\|x(t)\| \le \|X(0)\|\kappa_c e^{-\frac{\alpha_d}{NT}t}, \quad \forall t \ge 0, \qquad \|x_k(q)\| \le \|X(0)\|\kappa_c e^{-\alpha_d q}, \quad q = 0, 1, 2, \ldots \tag{12}$$

for any $X(0) = [x(0)^T, x_k(0)^T]^T$
Proof : Substituting $t = qNT$ and $\kappa_c = \kappa_d$, we obtain (11) straightforwardly from (12). Conversely, to derive (12) from (11), we can apply the proof of Theorem 3.1 in Ito *et al.* (1994) to (11). Equation (12) is found to be satisfied with $\kappa_c = \kappa_d e^{\alpha_d + \|A\|NT}$.

In Fig.1, we consider two pairs of exogenous input and output to take account of signals with different characteristics. Namely, we consider, for example, a situation where w_1 is a disturbance which dominates in high frequencies and w_2 is a signal in low frequencies. Let

$$\mathcal{T} = \begin{bmatrix} \mathcal{T}_{11} & \mathcal{T}_{12} \\ \mathcal{T}_{21} & \mathcal{T}_{22} \end{bmatrix} = \mathcal{F}_\ell(\boldsymbol{G}, \mathcal{HC}\,\mathcal{S}) \tag{13}$$

denote the closed loop map from the disturbance input $w := [w_1^T, w_2^T]^T$ to the controlled output $z := [z_1^T, z_2^T]^T$, where $\mathcal{T}_{ij}$ denotes the operator from w_j to z_i with zero initial conditions. This paper considers the following multirate sampled-data $\mathcal{H}^\infty$ control problem with two objectives subject to a decay rate constraint.

Problem 1 *Find a multirate controller* $\boldsymbol{C}$ *which continuous-time internally stabilizes the plant* $\boldsymbol{G}$ *and satisfies prescribed norm bounds*

$$\|\mathcal{T}_{11}\|_{\mathcal{B}(\mathcal{L}^2)} < 1 \quad \textit{and} \quad \|\mathcal{T}_{22}\|_{\mathcal{B}(\mathcal{L}^2)} < 1 \tag{14}$$

and a continuous-time decay rate α_c*, i.e.,*

$$\|x(t)\| \le \|X(0)\|\kappa_c e^{-\alpha_c t} \ ; \ \forall t \ge 0, \quad \|x_k(q)\| \le \|X(0)\|\kappa_c e^{-\alpha_c qNT} \ ; \ \forall q = 0, 1, 2, \ldots \tag{15}$$

A complete solution to Problem 1 is not known at the present time.

3 Norm preserving transformation

This section derives state-space formulas of a norm preserving transformation to evaluate continuous-time performance with two objectives and the transition decay rate. We will show how to construct a system $\acute{\boldsymbol{G}}$ which is called the discrete-time equivalent plant. The main theorem will be stated after that.

To begin with, we temporarily consider the single-objective version of multirate sampled-data $\mathcal{H}^\infty$ control. In this single-objective case, we are interested in a discrete-time system $\acute{\boldsymbol{G}}$ for which the following two statements are equivalent.

(T1) $\Sigma[\boldsymbol{G}, \mathcal{H}\boldsymbol{C}\mathcal{S}]$ is continuous-time internally stable and $\|\mathcal{T}\|_{\mathcal{B}(\mathcal{L}^2)} < 1$.

(T2) $\Sigma[\acute{\boldsymbol{G}}, \hat{\boldsymbol{C}}]$ is discrete-time internally stable and $\|\acute{\mathcal{T}}\|_\infty < 1$.

Here, $\mathcal{T} = \mathcal{F}_\ell(\boldsymbol{G}, \mathcal{H}\boldsymbol{C}\mathcal{S})$ and $\mathcal{S}$, $\mathcal{H}$, $\boldsymbol{G}$ and $\boldsymbol{C}$ are defined with (1) (2) (3), (4) and (8). The shift-invariant system $\acute{\boldsymbol{G}}$ achieving the equivalence is obtained through the following steps.

Step 1: Compute $\hat{B}_2, \hat{C}_2$ and $\hat{A}'$ which are defined by

$$\hat{B}_2 = \begin{bmatrix} \hat{B}_2(1,1) & \cdots & \hat{B}_2(1,m) \\ \vdots & \ddots & \vdots \\ \hat{B}_2(N+1,1) & \cdots & \hat{B}_2(N+1,m) \end{bmatrix}$$

$$[\hat{B}_2(i,j)]_h = \begin{cases} 0 & \\ & \text{if } i \le (h-1)K_j + 1 \\ \displaystyle\sum_{q=1}^{(i-1)-(h-1)K_j} e^{A[(i-1)-(h-1)K_j-q]T} \hat{B}_2(j) & \\ & \text{if } (h-1)K_j + 1 < i < hK_j + 1 \\ \displaystyle\sum_{q=1}^{K_j} e^{A[(i-1)-(h-1)K_j-q]T} \hat{B}_2(j) & \\ & \text{if } hK_j + 1 \le i \end{cases}$$

$$\hat{B}_2(i,j) = [[\hat{B}_2(i,j)]_1, [\hat{B}_2(i,j)]_2, \cdots, [\hat{B}_2(i,j)]_{M_j}]$$

$$\hat{B}_2(j) := \int_0^T e^{A\tau} d\tau B_{2,j}, \quad \hat{C}_2(i,j) = \begin{bmatrix} [\hat{C}_2(i,j)]_1 \\ [\hat{C}_2(i,j)]_2 \\ \vdots \\ [\hat{C}_2(i,j)]_{P_i} \end{bmatrix}$$

$$\hat{C}_2 = \begin{bmatrix} \hat{C}_2(1,1) & \cdots & \hat{C}_2(1,N+1) \\ \vdots & \ddots & \vdots \\ \hat{C}_2(p,1) & \cdots & \hat{C}_2(p,N+1) \end{bmatrix}, \qquad \hat{A}' = \begin{bmatrix} I \\ e^{AT} \\ \vdots \\ e^{ANT} \end{bmatrix}$$

$$[\hat{C}_2(i,j)]_r = \begin{cases} C_{2,i} & \text{if } j - 1 = (r-1)L_i \\ 0 & \text{otherwise} \end{cases} .$$

Step 2: Compute $W_\gamma := \int_0^T e^{A_V^T \tau} C_V^T C_V e^{A_V \tau} d\tau$ using

$$\int_0^T e^{A_V^T \tau} C_V^T C_V e^{A_V \tau} d\tau = \Phi_W^T \Gamma_W \quad ,$$

$$\begin{bmatrix} * & \Gamma_W \\ 0 & \Phi_W \end{bmatrix} = \exp\left\{ \begin{bmatrix} -A_V^T & C_V^T C_V \\ 0 & A_V \end{bmatrix} T \right\}$$

$$A_V = \begin{bmatrix} A & -B_1 B_1^T/\gamma & B_2 \\ C_1^T C_1/\gamma & -A^T & C_1^T D_{12}/\gamma \\ 0 & 0 & 0 \end{bmatrix},\ C_V = [0 \ \ -B_1^T \ 0].$$

Step 3: Calculate

$$\hat{B}_{1i} = e^{AiT} C_B e^{A_B T} B_B\ , \qquad i = 0, 1, \ldots, N-1\ ,$$

$$A_B = \begin{bmatrix} A & B_1 C_V/\gamma \\ 0 & A_V \end{bmatrix},\ B_B = \begin{bmatrix} 0 \\ W_\gamma^{-1/2} \end{bmatrix},\ C_B = [\, I_n \ 0\,]\ .$$

Step 4: Compute $\hat{M}_\gamma = \Phi_N^T \Gamma_N$ and $M_\gamma = B_N^T \hat{M}_\gamma B_N$ where

$$\begin{bmatrix} * & \Gamma_N \\ 0 & \Phi_N \end{bmatrix} = \exp\left\{ \begin{bmatrix} -A_N^T & C_N^T C_N \\ 0 & A_N \end{bmatrix} T \right\}\ ,$$

$$A_N = \begin{bmatrix} A & B_1 C_V/\gamma & B_2 \\ 0 & A_V & 0 \\ 0 & 0 & 0 \end{bmatrix},\ B_N = \begin{bmatrix} I & 0 & 0 \\ 0 & W_\gamma^{-1/2} & 0 \\ 0 & 0 & I \end{bmatrix},\ C_N = [\, C_1 \ 0 \ D_{12}\,].$$

Step 5: Obtain $\hat{C}_{10}$, $\hat{D}_0$, $\hat{D}_{12}$ from the equation $M_\gamma^{1/2} = [\hat{C}_{10},\ \hat{D}_0,\ \hat{D}_{e12}]$ and $\hat{D}_{12}(i) = \hat{D}_{e12} \bar{H}((i-1)T)$. Here, $\bar{H}(t)$ represents a zero-order hold function in the lifted domain, which is defined by

$$\bar{H}(t) = \begin{bmatrix} \mathbf{1}_1(t) & & 0 \\ & \mathbf{1}_2(t) & \\ & & \ddots \\ 0 & & \mathbf{1}_m(t) \end{bmatrix}$$

$$\mathbf{1}_j(t) = [\mathbf{1}_{j1}(t) \quad \mathbf{1}_{j2}(t) \ \cdots \ \mathbf{1}_{jM_j}(t)]\ ,$$

$$\mathbf{1}_{jl}(t) = \begin{cases} I_{f_j} & t \in [kNT + (l-1)K_j T,\ kNT + lK_j T), \\ 0 & \text{otherwise}\ , \end{cases}$$

where k is any nonnegative integer and $l = 1, 2, \ldots, M_j$.

Step 6: Calculate the following matrices.

$$\hat{C}_1 = \begin{bmatrix} \hat{C}_{10} & & 0 & 0 \\ & \ddots & & \vdots \\ 0 & & \hat{C}_{10} & 0 \end{bmatrix},\ \hat{D}_{11} = \begin{bmatrix} \hat{D}_0 & & 0 \\ & \ddots & \\ 0 & & \hat{D}_0 \end{bmatrix},$$

$$\hat{D}_{12} = \begin{bmatrix} \hat{D}_{12}(1) \\ \hat{D}_{12}(2) \\ \vdots \\ \hat{D}_{12}(N) \end{bmatrix},\ \hat{B}_1 = \begin{bmatrix} 0 & \cdots & \cdots & 0 \\ \hat{B}_{10} & 0 & \cdots & 0 \\ \hat{B}_{11} & \hat{B}_{10} & 0 & \vdots \\ \vdots & \ddots & \ddots & \ddots \\ \hat{B}_{1\,(N-1)} & \cdots & \hat{B}_{11} & \hat{B}_{10} \end{bmatrix}\ .$$

Step 7: Compute $\acute{B}_1, \acute{C}_1, \acute{D}_{11}, \acute{D}_{12}$ and $\acute{D}_{21}$ defined by

$$\acute{B}_1 = [\hat{B}_{1(N-1)} \ \cdots \ \hat{B}_{11} \ \hat{B}_{10}] \ , \quad \acute{C}_1 = \hat{C}_1 \hat{A}'$$
$$\acute{D}_{11} = \hat{D}_{11} + \hat{C}_1 \hat{B}_1 \ , \ \acute{D}_{12} = \hat{D}_{12} + \hat{C}_1 \hat{B}_2 \ , \ \acute{D}_{21} = \hat{C}_2 \hat{B}_1 \ .$$

Step 8: $\acute{A}, \acute{B}_2, \acute{C}_2, \acute{D}_{22}$ are given by

$$\acute{A} = e^{ANT}, \quad \acute{B}_2 = [\hat{B}_2(N+1,1) \ \cdots \ \hat{B}_2(N+1,m)]$$
$$\acute{C}_2 = \hat{C}_2 \hat{A}', \quad \acute{D}_{22} = \hat{C}_2 \hat{B}_2 \ .$$

Step 9: Finally, the equivalent system $\acute{\boldsymbol{G}}$ is obtained as

$$\acute{\boldsymbol{G}} = \left[\begin{array}{c|cc} \acute{A} & \acute{B}_1 & \acute{B}_2 \\ \hline \acute{C}_1 & \acute{D}_{11} & \acute{D}_{12} \\ \acute{C}_2 & \acute{D}_{21} & \acute{D}_{22} \end{array}\right] = \left[\begin{array}{cc} \acute{\boldsymbol{G}}_{11} & \acute{\boldsymbol{G}}_{12} \\ \acute{\boldsymbol{G}}_{21} & \acute{\boldsymbol{G}}_{22} \end{array}\right] \tag{16}$$

For the sake of brevity, the idea and details of driving this norm-preserving transformation for the single-objective problem are omitted since the complicated proof certainly takes up a lot of space and it is essentially similar to Kabamba and Hara (1993). The added difficulty is that, for a system given with multirate signals, we must define the hybrid state space representation which is easy of handling. The complex nature of the input-output relation also makes a difficulty of discretizing the controlled output. It might be better to mention that, when seeking the equivalent system, we utilized the discrete-time lifting in calculating an adjoint system and an equivalent of the worst case disturbance, and that we introduced an idea of using a nonstandard and nonminimal description of the system in order to reduce the complexity of the input-output relation and to minimize required computational tasks.

Now, we are ready to return to the multi-objective problem. In order to extend the above transformation technique to the two-objective case, we need to construct two pairs of exogenous input and output matrices. More precisely, it is required to carry out Step 2 to Step 7 for each $\mathcal{T}_{ii}$, $i = 1, 2$. Let

$$\left[\begin{array}{c|cc} \acute{A} & \acute{B}_1^i & \acute{B}_2 \\ \hline \acute{C}_1^i & \acute{D}_{11}^i & \acute{D}_{12}^i \\ \acute{C}_2 & \acute{D}_{21}^i & \acute{D}_{22} \end{array}\right] = \left[\begin{array}{cc} \acute{\boldsymbol{G}}_{11}^{\ i} & \acute{\boldsymbol{G}}_{12}^{\ i} \\ \acute{\boldsymbol{G}}_{21}^{\ i} & \acute{\boldsymbol{G}}_{22} \end{array}\right] = \acute{\boldsymbol{G}}^{\,i} \tag{17}$$

denote the single-objective discrete-time equivalent of the continuous-time system

$$\left[\begin{array}{c|cc} A & B_1^i & B_2 \\ \hline C_1^i & D_{11}^{ii} & D_{12}^i \\ C_2 & 0 & 0 \end{array}\right] = \left[\begin{array}{cc} \boldsymbol{G}_{11}^i & \boldsymbol{G}_{12}^i \\ \boldsymbol{G}_{21}^i & \boldsymbol{G}_{22} \end{array}\right] = \boldsymbol{G}^{\,i} \tag{18}$$

defined for the i-th objective. Namely,

$$\mathcal{T}_{ii} = \mathcal{F}_\ell(\boldsymbol{G}^i, \mathcal{HCS}), \quad i = 1,2 \tag{19}$$

holds. It should be noted that the quartet $(\acute{A}, \acute{B}_2, \acute{C}_2, \acute{D}_{22})$ is nothing but the discrete-time lifting representation of $(A, B_2, C_2, 0)$, and it is obvious that $\acute{D}_{22}$ satisfies (P_i, M_j)-causality conditions. Therefore, the two realizations of $\acute{\boldsymbol{G}}_{22}$ obtained for the two objectives case are identical so that we can combine the two realizations as

$$\acute{\boldsymbol{G}} = \left[\begin{array}{c|ccc} \acute{A} & \acute{B}_1^1 & \acute{B}_1^2 & \acute{B}_2 \\ \hline \acute{C}_1^1 & \acute{D}_{11}^1 & 0 & \acute{D}_{12}^1 \\ \acute{C}_1^2 & 0 & \acute{D}_{11}^2 & \acute{D}_{12}^2 \\ \acute{C}_2 & \acute{D}_{21}^1 & \acute{D}_{21}^2 & \acute{D}_{22} \end{array}\right] = \left[\begin{array}{ccc} \acute{\boldsymbol{G}}_{11}^1 & * & \acute{\boldsymbol{G}}_{12}^1 \\ * & \acute{\boldsymbol{G}}_{11}^2 & \acute{\boldsymbol{G}}_{12}^2 \\ \acute{\boldsymbol{G}}_{21}^1 & \acute{\boldsymbol{G}}_{21}^2 & \acute{\boldsymbol{G}}_{22} \end{array}\right] \tag{20}$$

where $*$ denotes appropriate transfer matrices. The system $\acute{\boldsymbol{G}}$ defined here is a causal, finite-dimensional linear shift-invariant discrete-time system. Let $\Sigma[\acute{\boldsymbol{G}}, \hat{\boldsymbol{C}}]$ denote a discrete-time closed-loop system shown in Fig.3. Define linear shift-invariant operators $\acute{\mathcal{T}}_{ij}$, $i, j = 1, 2$ by

$$\acute{z} = \left[\begin{array}{c} \acute{z}_1 \\ \acute{z}_2 \end{array}\right] = \acute{\mathcal{T}}\,\acute{w} = \left[\begin{array}{cc} \acute{\mathcal{T}}_{11} & \acute{\mathcal{T}}_{12} \\ \acute{\mathcal{T}}_{21} & \acute{\mathcal{T}}_{22} \end{array}\right] \left[\begin{array}{c} \acute{w}_1 \\ \acute{w}_2 \end{array}\right] . \tag{21}$$

Recall that $\boldsymbol{C}$ belongs to $\mathcal{L}_{SV}(M_j, P_i)$ and $\boldsymbol{C} = W_M^{-1} \hat{\boldsymbol{C}} W_P$ so that the direct-feedthrough matrix of the FDLSI system $\hat{\boldsymbol{C}}$ satisfies (M_j, P_i)-causality conditions. Then, we have the following theorem.

Theorem 3 *Consider the multirate sampled-data system $\Sigma[\boldsymbol{G}, \mathcal{H}\boldsymbol{C}\mathcal{S}]$ shown in Fig.1. Suppose that α_c and κ_c are positive real numbers. Then, the following are equivalent.*

(i) *$\Sigma[\boldsymbol{G}, \mathcal{H}\boldsymbol{C}\mathcal{S}]$ is continuous-time internally stable and satisfies*

$$\|x(t)\| \le \|X(0)\| \kappa_c e^{-\alpha_c t} \ ; \ \forall t \ge 0, \quad \|x_k(q)\| \le \|X(0)\| \kappa_c e^{-\alpha_c q NT} \ ; \ \forall q = 0, 1, 2, \ldots \tag{22}$$

Moreover, $\|\mathcal{T}_{11}\|_{\mathcal{B}(\mathcal{L}^2)} < 1$ and $\|\mathcal{T}_{22}\|_{\mathcal{B}(\mathcal{L}^2)} < 1$ are hold.

(ii) *$\Sigma[\acute{\boldsymbol{G}}, \hat{\boldsymbol{C}}]$ is discrete-time internally stable and has all the closed-loop poles in the closed disc with radius $e^{-\alpha_c NT}$ and center at origin in z-domain. Moreover, $\|\acute{\mathcal{T}}_{11}\|_\infty < 1$ and $\|\acute{\mathcal{T}}_{22}\|_\infty < 1$ are hold.*

Proof : Since $\acute{\boldsymbol{G}}^i$ for each $\mathcal{T}_{ii}$, $i = 1, 2$ guarantees the equivalence between **(T1)** and **(T2)** in terms of each objective, it is straightforward to see that the transformation from $\boldsymbol{G}$ to $\acute{\boldsymbol{G}}$ in (20) preserves multiple $\mathcal{L}^2$-induced norms of the two operators. It can be verified that the quartet $(\acute{A}, \acute{B}_2, \acute{C}_2, \acute{D}_{22})$ of the multi-objective equivalent $\acute{\boldsymbol{G}}$ is a state-space realization of the FDLSI system $W_P \mathcal{S} G_{22} \mathcal{H} W_M^{-1}$. Therefore, $\Sigma[\acute{\boldsymbol{G}}, \hat{\boldsymbol{C}}]$ has all the closed-loop poles in the closed disc of radius $e^{-\alpha_c NT}$ if and only if there exists a positive real number κ_d such that the state transition with $\acute{w} \equiv 0$ satisfies

$$\|\acute{x}(q)\| \le \|\acute{X}(0)\| \kappa_d e^{-\alpha_c NTq}, \quad \|x_k(q)\| \le \|\acute{X}(0)\| \kappa_d e^{-\alpha_c NTq}, \ \ \forall q = 0, 1, 2, \ldots \tag{23}$$

for any initial state $\acute{X}(0) = [\acute{x}(0)^T, x_k(0)^T]^T$. Here, $\acute{x}$ denotes the state variable of $\acute{\boldsymbol{G}}$. From $\acute{x}(q) = x(qNT)$ and Theorem 2 it follows that (23) is identical with (22). This concludes the proof.

Remark 1 *One might expect that Theorem 3 is considered as a multi-objective version of results in Voulgaris and Bamieh (1993) and Chen and Qiu (1994). However, it is not. Theorem 3 of this paper takes the same idea as Kabamba and Hara (1993) which has been developed for single-objective single-rate control and it is different from their ideas in two abovementioned papers. The combination in (20) is not successful if the approach in Voulgaris and Bamieh (1993) is adopted because of the loop shifting transformation which alters the state space completely with respect to the measurement output, control input and state. Voulgaris and Bamieh (1993) has to remove the operator mapping the continuous-time input to the continuous-time output by using the loop shifting technique, while in our approach the operator is taken into account directly in discretization of the controlled output. Moreover, since the method in Voulgaris and Bamieh (1993) affects the system, the decay rate is not preserved either. The drawback of using the loop shifting in discretization was also pointed out for single-rate systems in Hayakawa* et al. *(1994) and Fujioka* et al. *(1994). It also should be noted that the approach proposed by Chen and Qiu (1994) has the option of using the $\mathcal{H}^\infty$ discretization of Hayakawa* et al. *(1994) which does not affect the subsystem $\boldsymbol{G}_{22}$.*

4 Controller synthesis

The norm-preserving transformation developed in Section 3 reduces the original control problem to a multi-objective control problem of a pure discrete-time system. The following approach based on bilinear transformation and LMIs is proposed to solve the discrete-time $\mathcal{H}^\infty/\mathcal{H}^\infty$ control problem with a pole placement constraint stated in **(ii)** of Theorem 3.

Algorithm 1

Step 1: Obtain a two-objective equivalent $\acute{\boldsymbol{G}}$ from an original plant $\boldsymbol{G}$ with two objectives by following the procedure in Section 3 and (20).

Step 2: Define

$$E(z) = \acute{\boldsymbol{G}}(z) \begin{bmatrix} I & 0 \\ 0 & \frac{1}{z} I_M \end{bmatrix} .$$

Step 3: Let $\bar{E}(s) = E\left(\dfrac{2+\beta s}{2-\beta s}\right)$.

Step 4: Find a controller $\bar{F}(s)$ such that
1) $\Sigma[\bar{E}, \bar{F}]$ is internally stable;
2) $\|[\mathcal{F}_\ell(\bar{E}, \bar{F})]_{11}\|_\infty < 1$ and $\|[\mathcal{F}_\ell(\bar{E}, \bar{F})]_{22}\|_\infty < 1$,
where $\acute{\mathcal{T}} = \mathcal{F}_\ell(\bar{E}, \bar{F})$ and

$$\begin{bmatrix} \acute{z}_1 \\ \acute{z}_2 \end{bmatrix} = \begin{bmatrix} [\mathcal{F}_\ell(\bar{E}, \bar{F})]_{11} & [\mathcal{F}_\ell(\bar{E}, \bar{F})]_{12} \\ [\mathcal{F}_\ell(\bar{E}, \bar{F})]_{21} & [\mathcal{F}_\ell(\bar{E}, \bar{F})]_{22} \end{bmatrix} \begin{bmatrix} \acute{w}_1 \\ \acute{w}_2 \end{bmatrix} .$$

3) All poles of $\Sigma[\bar{E}, \bar{F}]$ are in the closed disc $\mathcal{D}$ with center at $(c, 0)$ and radius d :

$$c = \frac{2(e^{-2\alpha_c NT} + 1)}{\beta(e^{-2\alpha_c NT} - 1)} , \quad d = \frac{-4e^{-\alpha_c NT}}{\beta(e^{-2\alpha_c NT} - 1)}$$

Step 5: Define $F(z) = \bar{F}\left(\dfrac{2(z-1)}{\beta(z+1)}\right)$.

Step 6: Let $\hat{\boldsymbol{C}}(z) = \dfrac{1}{z}F(z)$.

Step 7: Then $\boldsymbol{C} = W_M^{-1}\hat{\boldsymbol{C}}W_P$ *is the multirate controller.*

Here, $\beta > 0$ is an arbitrary real number. The multirate sampled-data controller $\mathcal{H}W_M^{-1}\hat{\boldsymbol{C}}W_P\mathcal{S}$ is easily implemented with $\hat{\boldsymbol{C}}$ and parallelizing and deparallelizing calculators.

The controller $\boldsymbol{C}$ obtained by using Algorithm 1 is a solution to Problem 1. In fact, it is not difficult to verify that the bilinear transformation $s = \{2(z-1)\}/\{\beta(z+1)\}$ is bijective between the closed disc $\acute{\mathcal{D}}$ with radius $e^{-\alpha_c NT}$ and center at 0 in the z-plane and the disc $\mathcal{D}$ in the s-plane. Since the bilinear transformation preserves $\mathcal{H}^\infty$-norm, Theorem 3 implies that the existence of $\bar{F}(s)$ in Step 4 is sufficient for the existence of solutions to Problem 1. The condition is not necessary since the lifted controller $\hat{\boldsymbol{C}}(z)$ is restricted to be strictly proper. This restriction, however, guarantees that Algorithm 1 gives a causal multirate controller $\boldsymbol{C}$ belonging to $\mathcal{L}_{SV}(M_j, P_i)$. Compared with the design over all the (M_j, P_i)-causal controllers, Algorithm 1 may result in a conservative design on the one hand. On the other hand, due to this modification, the multi-objective problem with the pole-placement constraint in Step 4 of Algorithm 1 can be reduced to a convex optimization problem in terms of LMIs which is readily solvable.

The continuous-time $\mathcal{H}^\infty/\mathcal{H}^\infty$ output-feedback control problem with the pole-placement constraint in Step 4 can be solved using the LMI approach developed in Scherer *et al.* (1997). The concept of LMI region (Chilali and Gahinet, 1996; Gahinet *et al.*, 1995) can be used directly to represent the disc $\mathcal{D}$ for the pole placement constraint.

Remark 2 *If we use the single-objective transformation in Voulgaris and Bamieh (1993), we will have two different models for the individual objectives. The LMI approach to multi-objective output-feedback control such as Scherer* et al. *(1997) is not applicable to the multiple objectives expressed with multiple models. This illuminates the multi-objective transformation proposed in Section 3.*

Remark 3 *A tractable solution to the multi-objective and decay-rate constrained problem with (M_j, P_i)-causality conditions is not known at the present time although in the single-objective case, the decay-rate unconstrained problem with (M_j, P_i)-causality conditions has been solved by Chen and Qiu (1994). Therefore, this paper circumvented the difficulty of the (M_j, P_i)-causality by imposing strictly properness on $\hat{\boldsymbol{C}}$. It should be noted that the (M_j, P_i)-causality constraints on the controller in the synthesis cannot be represented by LMIs with respect to decision variables to solve. If $\hat{\boldsymbol{C}}$ is strictly proper, the controller $\boldsymbol{C}$ does not make any action for the initial NT seconds. In other words, $\boldsymbol{C}$ has an NT-delay element. This may limits achievable performance. However, at the same, time we should also aware that for real-time implementation controllers have to have some delay. In the single-rate case, strictly proper controllers are used commonly. This means that at least one T-delay element exists. In the multirate-case, a T-delay may be enough for real-time computation and NT is unnecessarily long in some fast loops. Nevertheless, the double cart example in Section 5 demonstrates that the performance achieved with a strictly proper $\hat{\boldsymbol{C}}$ is still good enough.*

5 Frequency dividing Cooperative Control

5.1 Double Cart System

Consider the double cart system (Sampei *et al.*, 1991) shown in Fig.4. The variable h_1 denotes the position of the lower cart measured from a certain initial point on the floor. The position of the upper cart measured relatively to the lower cart is denoted by h_2. Hence, the absolute position of the upper cart is $h = h_1 + h_2$. The control objective is to make the upper cart track the reference signal r. Error signals e and e_1 are defined by $e = r - h$ and $e_1 = r - h_1$. The control inputs of the double cart system are the forces f_1 and f_2 directly driving the lower cart and upper cart, respectively. For measurement signals, the error e and the cart positions h_1, h_2 are available. The mass M_1 of the lower cart is 4 kg. The mass M_2 of the upper cart is 0.4 kg so that the cart is more flexible and requires less amount of energy than the lower one to follow the reference signal. That is why we naturally prefer frequency dividing cooperative control(FDCC) in which the upper cart moves quickly and accurately while the lower cart moves slowly and roughly. In other words, when the reference r only contains signals of low frequencies, the lower cart should contributes to tracking. For reference signals in high frequencies, the upper cart moves to track the reference while the lower cart almost does not. The equations of motion of the double cart are

$$
\begin{aligned}
M_1\ddot{h}_1 + D_1\dot{h}_1 - D_2\dot{h}_2 &= f_1 - f_2 \\
M_2(\ddot{h}_1 + \ddot{h}_2) + D_2\dot{h}_2 &= f_2 \ ,
\end{aligned}
$$

where viscous friction coefficients are $D_1 = 20[N \cdot \sec/m]$ and $D_2 = 2[N \cdot \sec/m]$. $-f_2$ in the upper equation represents the reaction force from the upper cart to lower cart, i.e., for instance, the upper cart is driven by an electric motor whose stator is fixed to the lower cart. With all equations given in the above, a mapping from (r, f_1, f_2) to (e_1, h_1, h_2, e) is defined as a continuous-time FDLTI system which is denoted by $\boldsymbol{P}$.

Since the lower cart is supposed to act in low frequencies, the force signals f_1 may not need to have high frequency components and only low frequency components of h_1 may be important. On the other hand, high frequency components of h_2, e and f_2 are necessary since the upper cart should act in high frequencies. Therefore, we can expect that in order to synthesize a desired tracking control system with sampled-data controllers based on such an FDCC strategy, the period T_1 of sampling h_1 and holding f_1 can be larger than the period T_2 of sampling h_2, e and holding f_2. Figure 5 depicts the multirate control of the double cart system.

5.2 Controller Design

Now, consider the augmented system $\Sigma[\boldsymbol{G}, \mathcal{HCS}]$ shown in Fig.6 which gives a block diagram of the closed-loop control system. The stable FDLTI system W_1 is a low-pass filter representing the frequency band in which the lower cart should be driven. The FDLTI low-pass system W_2 has higher bandwidth to make the tracking error small by moving the upper cart at high frequencies. The stable FDLTI system W_i which has unit magnitude is also a low-pass filter representing the total frequency band of the reference signal r. The FDCC problem of the double cart system can be stated as follows:

Double cart control problem : Let $T_1 > T_2$. Find a multirate controller $\boldsymbol{C}$ which achieves

$$\min_{\boldsymbol{C}} \max \left\{ \|\mathcal{T}_{11}\|_{\mathcal{B}(\mathcal{L}^2)},\ \|\mathcal{T}_{22}\|_{\mathcal{B}(\mathcal{L}^2)} \right\} \tag{24}$$

subject to

- the closed-loop system is continuous-time internally stable.
- the decay rate α_c is greater than $-\ln(0.1) \approx 2.30$.

Here, $\mathcal{T}_{ii}$, $i = 1, 2$ denotes the map between w_i and z_i in Fig.6. Let the weighting functions be chosen as

$$W_i = \frac{100}{(s+10)^2}, \quad W_1 = \frac{0.07}{s+0.07}, \quad W_2 = \frac{5}{s+5} \ .$$

The min-max problem (24) is expressed alternatively by

$$\min_{\boldsymbol{C}} \gamma \qquad \text{subject to} \quad \|\frac{1}{\gamma}\mathcal{T}_{11}\|_{\mathcal{B}(\mathcal{L}^2)} < 1,\ \|\frac{1}{\gamma}\mathcal{T}_{22}\|_{\mathcal{B}(\mathcal{L}^2)} < 1 \ . \tag{25}$$

This problem can be readily solved by using Algorithm 1. The minimization is done by an iterative search of γ.

Before moving on to the controller design, we need to modify the decay-rate specification. According to Theorem 3, the decay rate constraint is identical with

- $\Sigma[\acute{\boldsymbol{G}}, \hat{\boldsymbol{C}}]$ has all closed-loop poles inside the closed disc $\acute{\mathcal{D}}$ defined with radius $e^{-\alpha_c NT}$ and center at origin in z-domain.

or equivalently,

- $\Sigma[\bar{E}, \bar{F}]$ has all closed-loop poles inside the closed disc $\mathcal{D}$ in s-domain.

Here, notice that the mode -0.07 of W_1 is not observable from (h_1, h_2, e). No controller can change the decay rate of the mode, which is against $\alpha_c > 2.30$. The system $\Sigma[\acute{\boldsymbol{G}}, \hat{\boldsymbol{C}}]$ will have a pole outside the closed disc, i.e., at $e^{-0.07NT}$. Remember that the system $\boldsymbol{G}$ is not the actual double cart system but an augmented one just for controller synthesis. Since the actual double cart is $\boldsymbol{P}$ which does not include W_1, the decay rate constraint should be applied to the state transition of the actual closed-loop system $\Sigma[\boldsymbol{P}, \mathcal{H}\boldsymbol{C}\mathcal{S}]$. This means that we can leave the mode -0.07 unchanged. For this purpose, the closed disc is modified to include the mode -0.07:

- $\Sigma[\acute{\boldsymbol{G}}, \hat{\boldsymbol{C}}]$ has all closed-loop poles inside the region $\acute{\mathcal{E}}$ in z-domain.

which is equivalent to

- $\Sigma[\bar{E}, \bar{F}]$ has all closed-loop poles inside $\mathcal{E}_1 \cap \mathcal{E}_2$:
  $\mathcal{E}_1$: Conic sector $\{(x, y) : y \geq kx, \quad y \leq -kx\}$
  $$k = \tan\left(\arcsin\left(\frac{2e^{-\alpha_c NT}}{e^{-2\alpha_c NT}+1}\right)\right)$$
  $\mathcal{E}_2$: Ellipsoid $\{(x, y) : ((x-c)/a)^2 + (y/b)^2 \leq 1\}$
  $$c = \frac{e^{-\alpha_c NT}+1}{\beta(e^{-\alpha_c NT}-1)}, \quad a = c, \quad b = \frac{-4e^{-\alpha_c NT}}{\beta(e^{-2\alpha_c NT}-1)}$$

Here, the closed set $\acute{\mathcal{E}}$ is defined such that $\mathcal{E}_1 \cap \mathcal{E}_2$ is the image of the bilinear transformation of $\acute{\mathcal{E}}$. Figure 7 shows the original region $\acute{\mathcal{D}}$(dashed line) and the modified region $\acute{\mathcal{E}}$(solid line). The dotted line is the unit circle and the location of the mode -0.07 in the plane is indicated by "o". We used this reasonable approximation $\mathcal{E}_1 \cap \mathcal{E}_2$ in Step 4 of Algorithm 1 instead of using $\mathcal{D}$.

Using Algorithm 1 together with the above modification of region, we designed controllers for the following three cases.

$$\begin{array}{lcl} \text{Fast single-rage case} & : & T_1 = 0.01[\text{sec}], \quad T_2 = 0.01[\text{sec}] \\ \text{Multi-rate case} & : & T_1 = 0.03[\text{sec}], \quad T_2 = 0.01[\text{sec}] \\ \text{Slow single-rage case} & : & T_1 = 0.03[\text{sec}], \quad T_2 = 0.03[\text{sec}] \end{array}$$

The $\mathcal{L}^2$-induced norm of two objective mappings and the decay rate are shown in Table 1. Note that $\mathcal{L}^2$-induced norms in Table 1 are the minimum values Algorithm 1 achieves, which are not guaranteed to be global optima. The decay rate α_c achieved was computed as $\alpha_c = -\ln(\alpha)/NT$, where α is the maximum absolute value of the poles of $\Sigma[\hat{\boldsymbol{P}}_{22}, \hat{\boldsymbol{C}}]$ (See Appendix A). Numerical data of a multirate controller $\boldsymbol{C}$ obtained is given in Appendix B. Sampled-data frequency responses (Yamamoto and Khargonekar, 1996; Araki *et al.*, 1996; Hara *et al.*, 1995; Yamamoto *et al.*, 1997) of the 0.03[sec]-periodic closed-loop system in the three cases are shown in Fig.8 and Fig.9 for each objective. Peak values over frequencies are the $\mathcal{L}^2$-induced norm of $\mathcal{T}_{ii}$, $i = 1, 2$. These plots indicate the aliasing effect when signals are sampled with the lower frequency. In consequence, the curves of sampled-data frequency responses in the slow single-rate case are pushed up a lot. These responses illustrate the differences among a multirate controller and single-rate controllers and it is seen that the multirate case makes a satisfactory compromise successfully. The poles of the multirate systems $\Sigma[\hat{\boldsymbol{P}}_{22}, \hat{\boldsymbol{C}}]$ obtained are plotted in Fig.7. All poles of the closed-loop are contained in $\acute{\mathcal{E}}$ and they are in $\acute{\mathcal{D}}$ as well. The time responses to sinusoid inputs in the multi-rate case are shown in Fig.10, Fig.11 and Fig.12. According to Fig.10, for the low frequency input $r = \sin 0.3t$, while the upper is almost at rest, the lower cart achieves nearly perfect tracking. In the case of the high frequency sinusoid $r = \sin 10t$ in Fig.12, the movement of the upper cart compensates the discrepancy between the reference signal and the lower cart successfully. For the middle frequency range $r = \sin 3t$, Fig.11 shows that the lower cart moves in cooperation with the upper cart to achieve a required level of tracking performance. Figure.13 shows the time response to a band limited step-type signal $r(t)$ given by

$$r(s) = F(s) r_s(s), \quad F(s) = \frac{10000}{(s+100)^2}, \quad r_s(t) = \begin{cases} 0 & \text{for} \quad 0 \le t < 0.1 \\ 1 & \text{for} \quad 0.1 \le t < 1 \\ 0 & \text{for} \quad 1 \le t \end{cases} . \tag{26}$$

The response illustrates the feature of an FDCC system and it is seen that the settling time is consistent with the decay rate we specified.

To make anther comparison, we also computed controllers by using a transform method which discretizes continuous-time controllers. A continuous-time controller was found as a solution to the continuous-time $\mathcal{H}^\infty/\mathcal{H}^\infty$ control problem. Then, it was transformed to a single-rate sampled-data controller with sampling period T by using the bilinear transformation $s = \{2(z-1)\}/\{T(z+1)\}$. Here, the $\mathcal{L}^2$-induced norm is identical with $\mathcal{H}^\infty$-norm of the transfer function when the controller is an FDLTI continuous-time system. The norms achieved in the continuous-time design were $\|\mathcal{T}_{11}\|_\infty = 4.7 \times 10^{-6}$ and $\|\mathcal{T}_{22}\|_\infty = 4.3 \times 10^{-7}$. The maximum

absolute values of discrete closed-loop poles of the resulting sampled-data system $\Sigma[\hat{\boldsymbol{P}}_{22}, \hat{C}]$ were 460.8 and 246.3 for sampling period $T = 0.01$ and $T = 0.03$, respectively. Although the norms are very small in continuous time, the discretized controllers does not stabilize the system at all.

The result in this section showed that it is important to select suitable periods of sampling and holding by taking account of frequency characteristics of systems and signals. By using multirate control and the idea of FDCC, we could avoid unnecessarily fast sampling and holding to obtain a tracking control system with a required level of accuracy.

6 Conclusions

This paper has discussed multi-objective control design of multirate sample-data systems. Explicit state-space formulas have been derived for an $\mathcal{L}^2$-induced norm preserving transformation of the multirate sample-data systems. These formulas are particularly suited for multi-objective control with pole placement constraints. Actually, they have been successfully used to suggest an approach to multi-objective multirate controller synthesis with decay rate specifications. Furthermore, we introduced the multi-objective multirate control design into frequency dividing cooperative control of systems having redundant degrees of freedom. The frequency dividing cooperative control is very useful in practical situations where there are several components, disturbances and perturbations which have diverse characteristics. The multi-objective approach to multirate systems proposed in this paper can be utilized to select suitable sampling and hold periods.

References

Araki, M., Y. Ito and T. Hagiwara (1996). Frequency response of sampled-data systems. *Automatica* **32**, 483–497.

Bamieh, B.A. and J.B. Pearson (1992). A general framework for linear periodic systems with application to sampled-data control. *IEEE Trans. Automat. Contr.* **37**, 418–435.

Chen, T. and L. Qiu (1994). $\mathcal{H}^\infty$ design of general multirate sampled-data control systems. *Automatica* **30**, 1139–1152.

Chilali, M. and P. Gahinet (1996). $\mathcal{H}^\infty$ design with pole placement constraints: An LMI approach. *IEEE Trans. Automat. Contr.* **41**, 358–367.

Franklin, G.F., J.D. Powell and M.L. Workman (1990). *Digital control of dynamic systems*. 2 ed.. Addison-Wesley Publishing Co.

Fujioka, H., S. Hara and H. Nakamura (1994). Mixed $\mathcal{H}^2/\mathcal{H}^\infty$ control for sampled-data feedback systems. In: *1st Asian Contr. Conf.*. Vol. 3. pp. 61–64.

Gahinet, P., A. Nemirovski, A.J. Laub and M. Chilali (1995). *LMI control toolbox*. The MathWorks Inc.

Glasson, D.P. (1983). Development and applications of multirate digital control. *IEEE Control Systems Magazine* **3**, 2–8.

Hara, S., H. Fujioka, P.P. Khargonekar and Y. Yamamoto (1995). Computational aspects of gain-frequency response for sampled-data systems. In: *34th IEEE Conf. Decision. Contr.* pp. 1788–1789.

Hayakawa, Y., S. Hara and Y. Yamamoto (1994). $\mathcal{H}^\infty$ type problem for sampled-data control systems– a solution via minimum energy characterization. *IEEE Trans. Automat. Contr.* **39**, 2278–2284.

Ito, H., H. Ohmori and A. Sano (1994). Stability analysis of multirate sampled-data control systems. *IMA J. Math. Contr. Inform.* **11**, 341–354.

Ito, H., H. Ohmori and A. Sano (1995). A subsystem design approach to continuous-time performance of decentralized multirate sampled-data systems. *Int. J. Systems. Sci.* **26**, 1263–1287.

Ito, H., T. Chuman, H. Ohmori and A. Sano (1996). An approach to multirate control design with multiple objectives. In: *13th IFAC World Congress.* Vol. C. pp. 325–330.

Kabamba, P.T. and S. Hara (1993). Worst-case analysis and design of sampled-data control systems. *IEEE Trans. Automat. Contr.* **38**, 1337–1357.

Meyer, D.G. (1990). A parametrization of stabilizing controllers for multirate sampled-data systems. *IEEE Trans. Automat. Contr.* **35**, 233–236.

Sampei, M., H. Itoh, T. Mita and Y. Ohyama (1991). $\mathcal{H}^\infty$ control of a plant with redundant degree of freedom. In: *'91 Korea Automat. Contr. Conf.*. pp. 1493–1496.

Scherer, C., P. Gahinet and M. Chilali (1997). Multiobjective output-feedback control via LMI optimization. *IEEE Trans. Automat. Contr.* **42**, 896–911.

Semba, T. (1993). Model-following digital servo using multirate sampling for an optical disk drive. *Japan J. Appl. Phys.* **32**, 5385–5391.

Sun, W., K. Nagpal, P.P. Khargonekar and K.R. Poolla (1992). Digital control systems: $\mathcal{H}^\infty$ controller design with zero-order hold function. In: *31st IEEE Conf. Decision. Contr.* pp. 475–480.

Teraoka, K., T. Ichiya and H. Ito (1997). Design of multirate tracking control systems with division of frequency bonds. In: *36th SICE Annual Conf.*. pp. 131–134. in Japanese.

Voulgaris, P.G. and B. Bamieh (1993). Optimal $\mathcal{H}^\infty$ and $\mathcal{H}^2$ control of hybrid multirate systems. *Syst. Contr. Lett.* **20**, 249–261.

Yamamoto, Y. (1994). A function space approach to sampled data control systems and tracking problems. *IEEE Trans. Automat. Contr.* **39**, 703–713.

Yamamoto, Y., A.G. Madievski and B.D.O. Anderson (1997). Computation and convergence of frequency response via fast sampling for sampled-data control systems. In: *36th IEEE Conf. Decision. Contr.* pp. 2157–2162.

Yamamoto, Y. and P.P. Khargonekar (1996). Frequency response of sampled-data systems. *IEEE Trans. Automat. Contr.* **41**, 166–176.

A Estimating decay rate

Now, let $(A_P, B_P, C_P, 0)$ denote the state space model of $\boldsymbol{P}$, where input and output matrices are given by

$$B_P = \begin{bmatrix} B_r & B_{f1} & B_{f2} \end{bmatrix}, \qquad C_P = \begin{bmatrix} C_{e1} \\ C_{h1} \\ C_{h2} \\ C_e \end{bmatrix}.$$

The unforced closed-loop system is represented by $\Sigma[\boldsymbol{P}_{22}, \mathcal{H}\boldsymbol{C}\mathcal{S}]$. Here,

$$\boldsymbol{P}_{22} := \left[\begin{array}{c|cc} A_P & B_{f1} & B_{f2} \\ \hline C_{h1} & 0 & 0 \\ C_{h2} & 0 & 0 \\ C_e & 0 & 0 \end{array}\right]$$

This state-space model is a reduced-order realization of $\boldsymbol{G}_{22}$, which is obtained by removing all modes of W_1, W_2 and W_i. The discrete-time lifted system of $\mathcal{S}\boldsymbol{P}_{22}\mathcal{H}$ is represented by $\hat{\boldsymbol{P}}_{22} = W_P \mathcal{S}\boldsymbol{P}_{22}\mathcal{H} W_M^{-1}$. Using argument similar to Theorem 3, it is easy to see that $\Sigma[\boldsymbol{P}, \mathcal{H}\boldsymbol{C}\mathcal{S}]$ has the continuous-time decay rate $\alpha_c > 0$ if and only if the poles of $\Sigma[\hat{\boldsymbol{P}}_{22}, \hat{\boldsymbol{C}}]$ has all poles in the closed disc $\acute{\mathcal{D}}$ defined with radius $e^{-\alpha_c NT}$ and center at the origin.

B A controller designed

A multirate controller $\boldsymbol{C} = W_M^{-1}\hat{\boldsymbol{C}}W_P$ with which the double cart system is continuous-time internally stable is given by

$$\hat{\boldsymbol{C}} = \left[\begin{array}{c|c} A_c & B_c \\ \hline C_c & D_c \end{array}\right],$$

where

$$A_c = \mathrm{diag}\left[0.019, -0.157, -0.375, \begin{bmatrix} 0.442 & -0.332 \\ 0.332 & 0.442 \end{bmatrix}, -0.624, -0.802, 0.829, 0.992, \begin{bmatrix} 2.216 & -0.535 \\ 0.535 & 2.216 \end{bmatrix}\right]$$

$$B_c = \begin{bmatrix} 8.28 & 4.4 & 4.06 & -1.36 & -4.07 & 5.1 & 5.41 \\ 85.3 & 49.9 & 44.0 & -33.6 & -33.4 & 75.5 & 48.7 \\ 136.5 & 83.2 & 84.2 & -40.34 & -54.3 & 100.6 & 102.5 \\ 2.07 & -0.71 & 2.46 & 12.05 & -9.99 & -15.35 & 11.07 \\ 10.16 & 1.57 & 0.14 & 10.97 & -15 & -8.25 & 7.85 \\ -36.9 & -24.56 & -26.7 & 10 & 12.61 & -26.1 & -32.72 \\ -13.12 & -7.83 & -9.19 & 2.25 & 6 & -6.75 & -12.38 \\ 0 & -1.99 & -6.49 & 2.09 & -9 & 0.01 & -5.83 \\ 0.03 & 1.65 & 0.83 & 0.34 & 1.17 & 0.64 & 0.54 \\ -66.2 & -52.9 & -92.3 & -280.2 & 170.9 & 271 & -269.4 \\ 48.2 & 45.6 & 89.4 & 192.5 & -108.9 & -195.3 & 219.1 \end{bmatrix}$$

$$C_c = \begin{bmatrix} -6.1 & -6.4 & 0.7 & -79.2 & -7.3 & 21.7 & -43.6 & 1.7 & 4.2 & -49.6 & -34.7 \\ 60.8 & 72.9 & -53.1 & 56.0 & -24 & -29.5 & -13.8 & -51.0 & 14.4 & -66.5 & -26.4 \\ 44.4 & 20.2 & -35.8 & -13.6 & 14.9 & -34 & -30.7 & 23.8 & -6.7 & 7.3 & -3 \\ -24.2 & 6.7 & -16.4 & -20.9 & 19.5 & -16.7 & -20.4 & 22.4 & -9.7 & 31.7 & 11.9 \end{bmatrix}$$

$$D_c = 0$$

This controller was obtained after model reduction of the 16th-order multirate controller computed in Table 1. The coefficients were rounded to the nearest numbers in short length . The controller given in the above achieves $\|\mathcal{T}_{11}\|_{\mathcal{B}(\mathcal{L}^2)} = 0.0039$ and $\|\mathcal{T}_{22}\|_{\mathcal{B}(\mathcal{L}^2)} = 0.0098$. The decay rate is $\alpha_c = 5.26$.

Table 1: $\mathcal{L}^2$-induced norm and decay rate achieved

	Fast single-rate	Multi-rate	Slow single-rate
$\|\mathcal{T}_{11}\|_{\mathcal{B}(\mathcal{L}^2)}$	0.0012	0.0037	0.0123
$\|\mathcal{T}_{22}\|_{\mathcal{B}(\mathcal{L}^2)}$	0.0024	0.0091	0.0371
Decay rate α_c	3.81	5.26	2.07

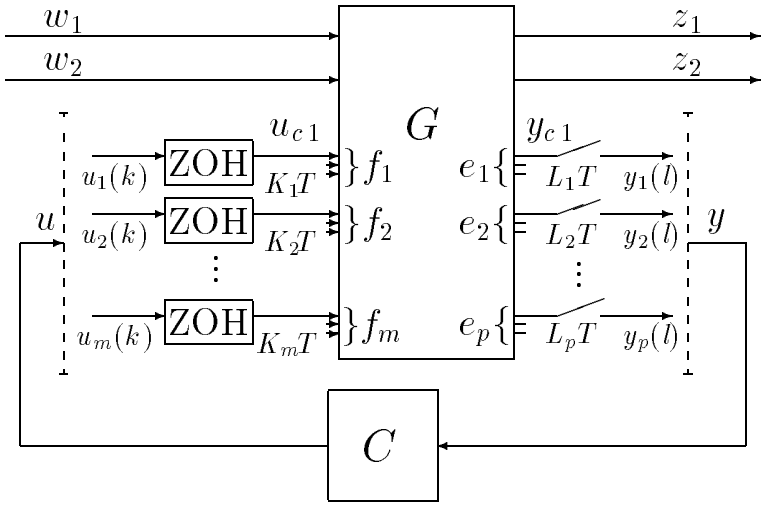

Figure 1: Multirate system with two objectives

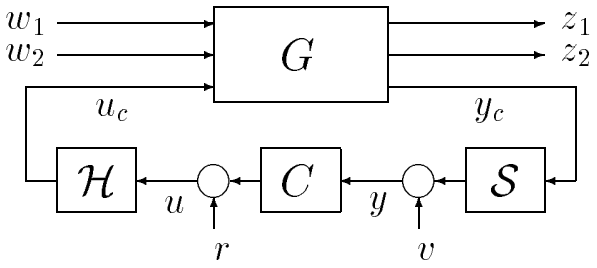

Figure 2: $\mathcal{L}^\nu$ hybrid stability

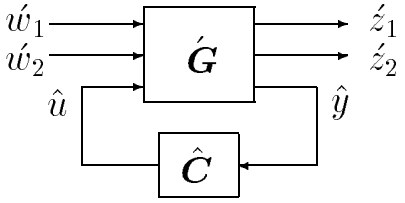

Figure 3: Equivalent discrete-time system

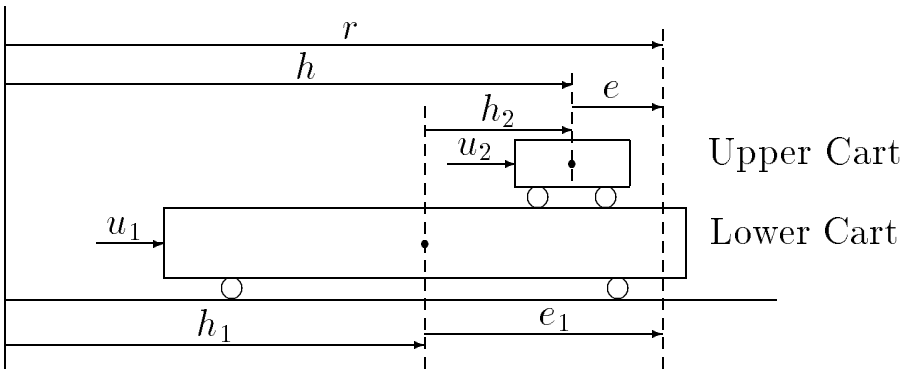

Figure 4: Dobuble cart system

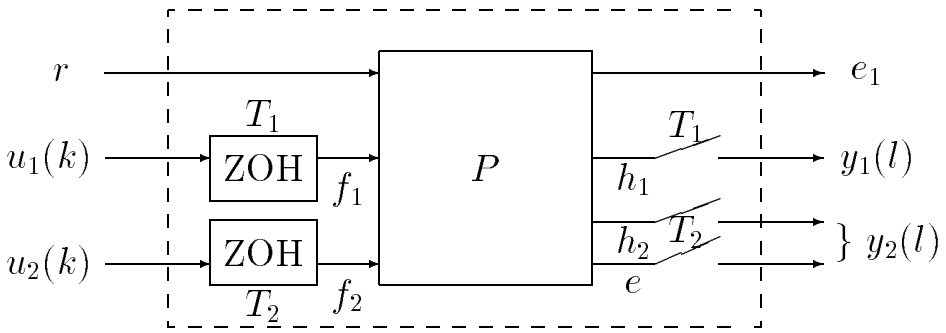

Figure 5: Multirate tracking control

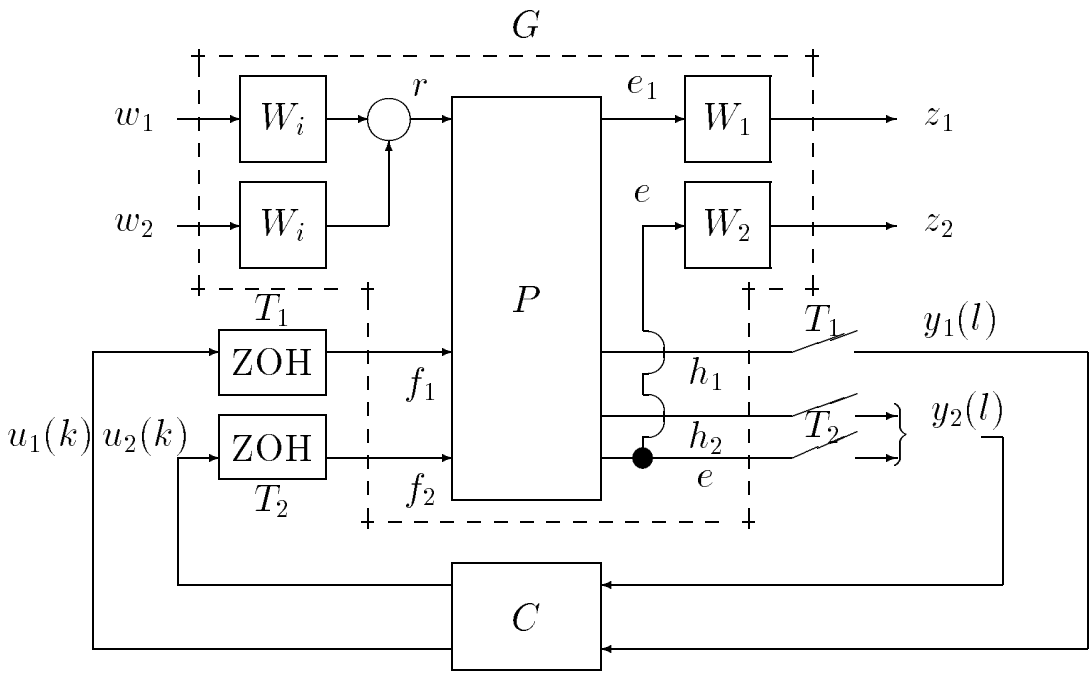

Figure 6: Frequency dividing cooperative control

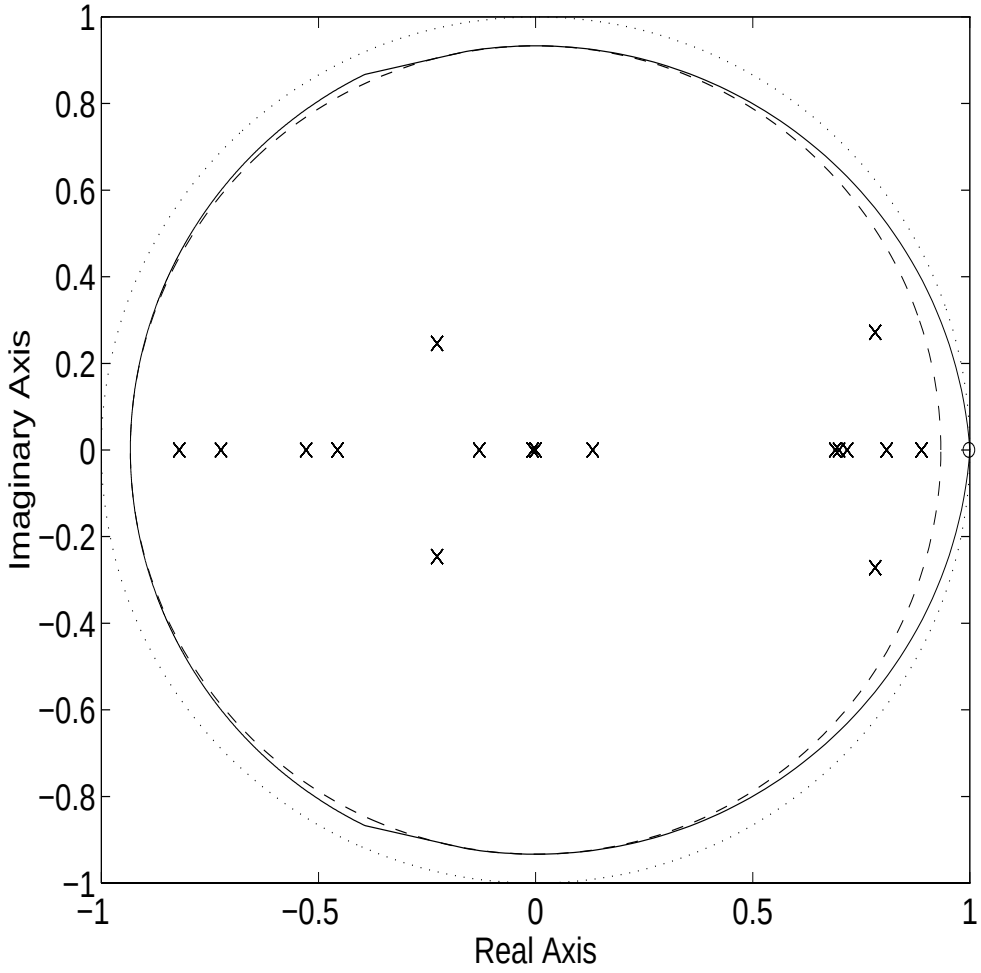

Figure 7: Specified region and closed-loop poles in z-domain:
Multi-rate case, $\beta = 0.007$
Modified region $\acute{\mathcal{E}}$ (solid); Original disc $\acute{\mathcal{D}}$ (dashed); Unit circle(dotted).

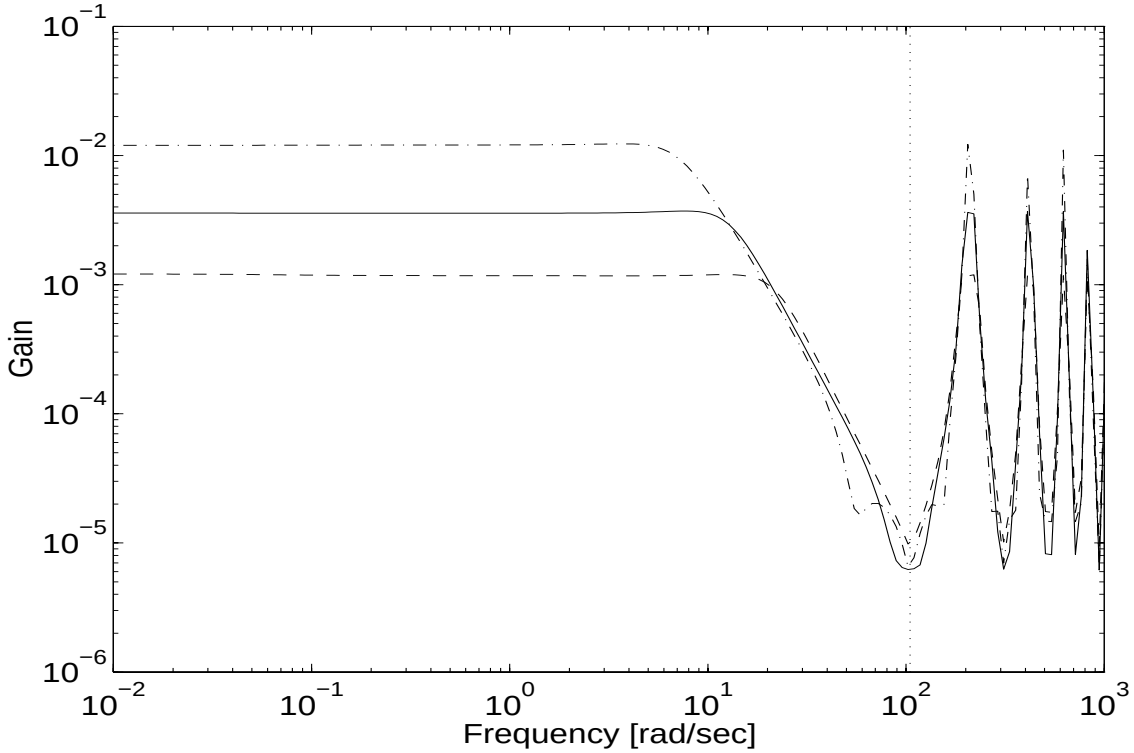

Figure 8: Sampled-data frequency response of $\mathcal{T}_{11}$:
Multirate(solid); Fast single-rate(dashed); Slow single-rate(dash-dot).

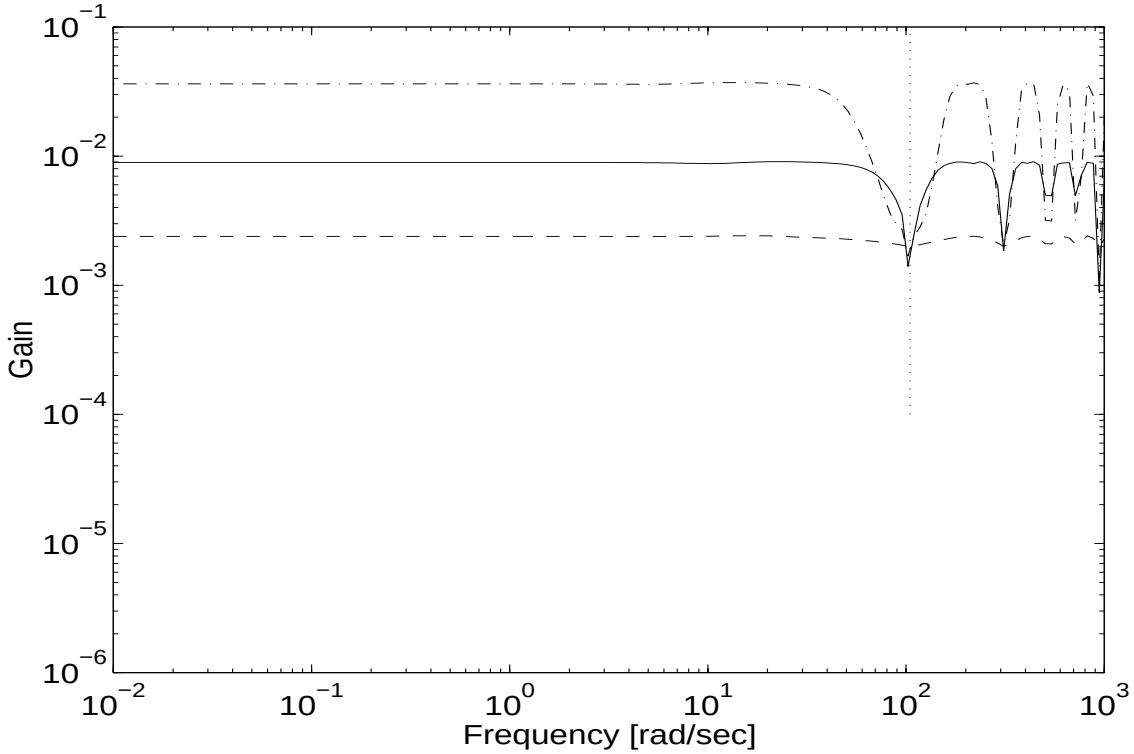

Figure 9: Sampled-data frequency response of $\mathcal{T}_{22}$:
Multirate(solid); Fast single-rate(dashed); Slow single-rate(dash-dot).

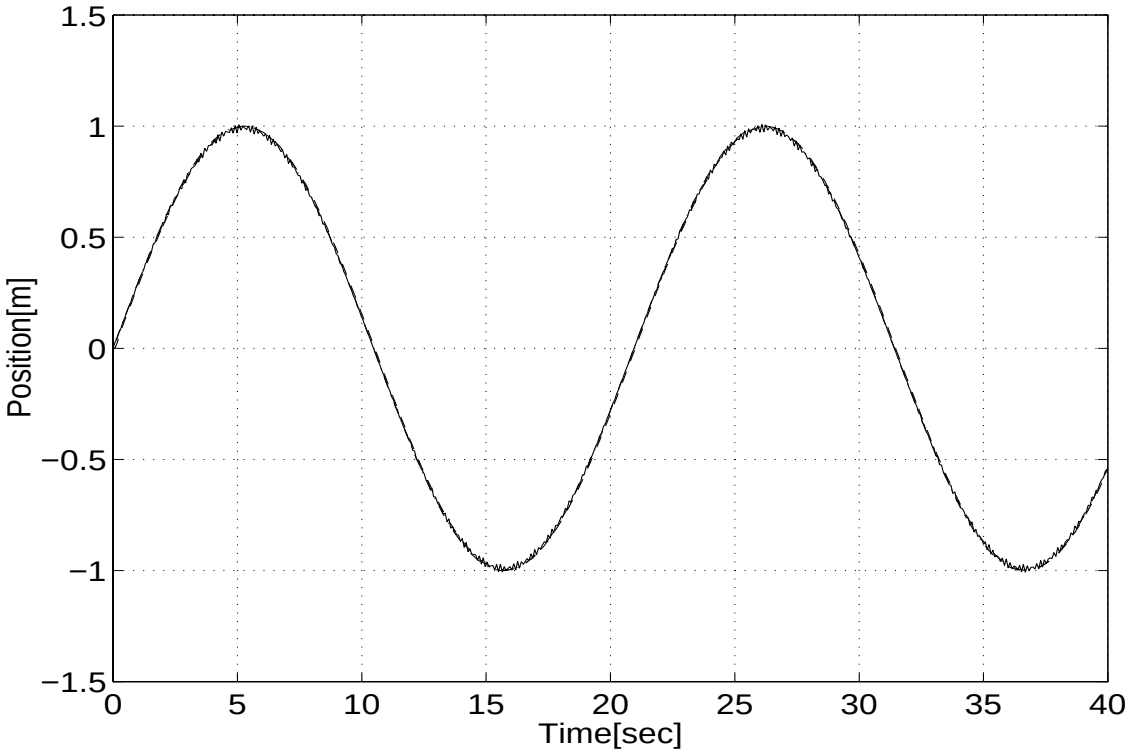

Figure 10: Reference $r = \sin 0.3t$ and response of two carts:
Lower cart h_1(dashed); Upper cart h(solid); Reference r(dash-dot).

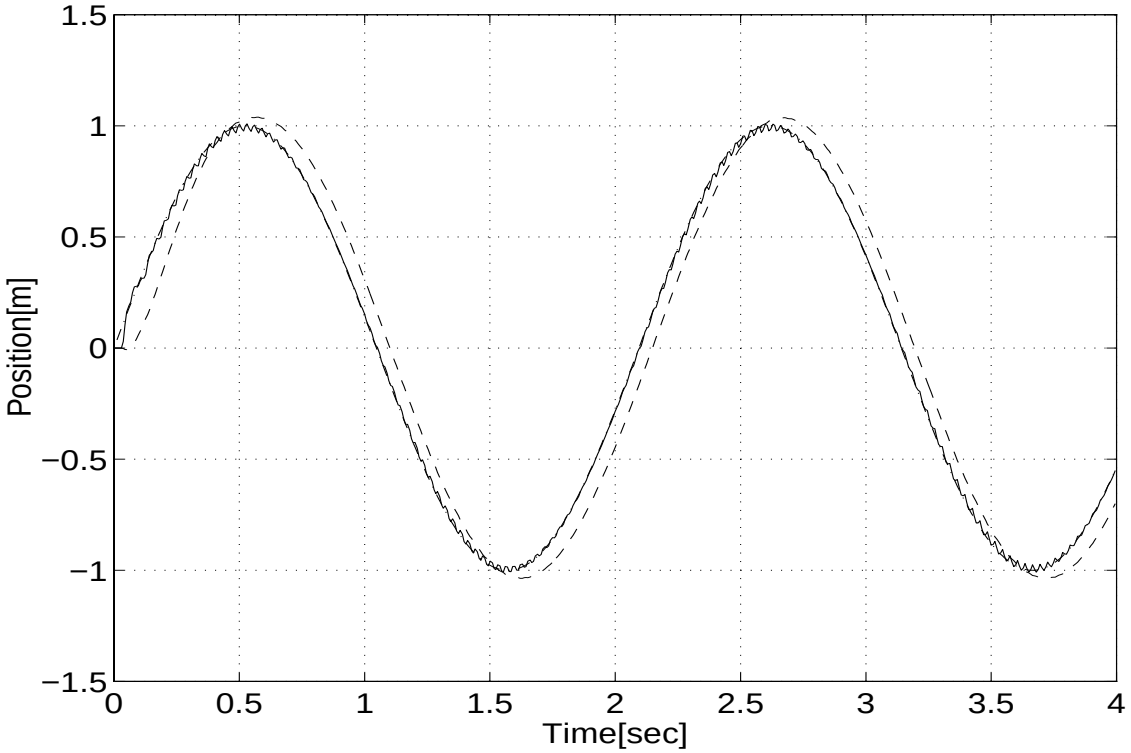

Figure 11: Reference $r = \sin 3t$ and response of two carts:
Lower cart h_1(dashed); Upper cart h(solid); Reference r(dash-dot).

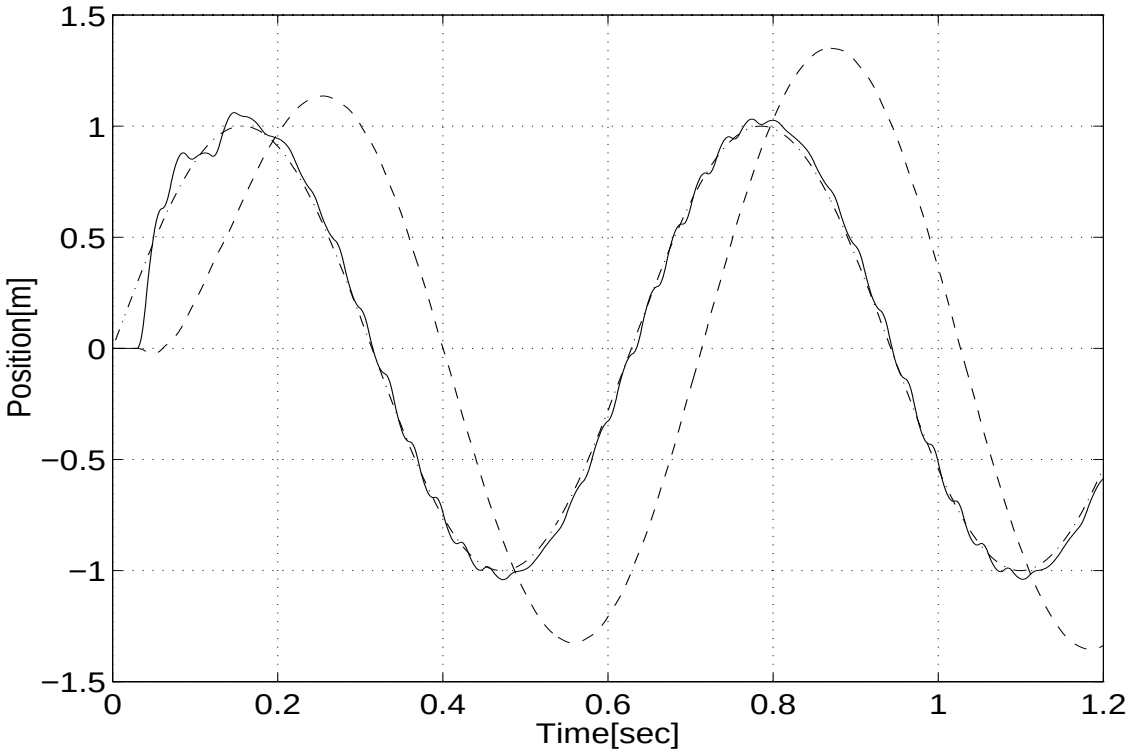

Figure 12: Reference $r = \sin 10t$ and response of two carts:
Lower cart h_1(dashed); Upper cart h(solid); Reference r(dash-dot).

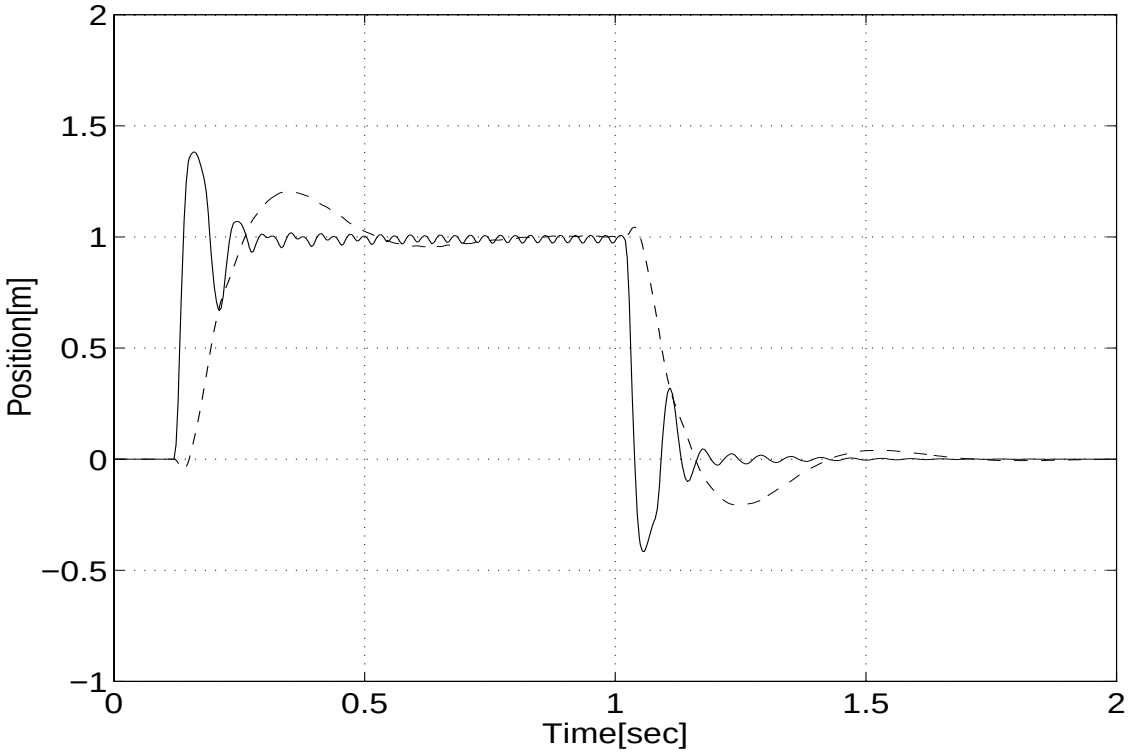

Figure 13: Reference signal and time response of two carts:
Lower cart h_1(dashed); Upper cart h(solid); Reference r(dash-dot).